

# Preparation of interconnected poly( $\epsilon$ -caprolactone) porous scaffolds by a combination of polymer and salt particulate leaching

Joël Reignier\*, Michel A. Huneault

*Industrial Materials Institute, National Research Council Canada, 75, de Mortagne, Boucherville, QC, Canada J4B 6Y4*

Received 4 January 2006; received in revised form 13 April 2006; accepted 18 April 2006

Available online 16 May 2006

## Abstract

This paper examines a new technique for the preparation of porous scaffolds by combining selective polymer leaching in a co-continuous blend and salt particulate leaching. In the first step of this technique, a co-continuous blend of two biodegradable polymers, poly( $\epsilon$ -caprolactone) (PCL) and polyethylene oxide (PEO), and a certain amount of sodium chloride salt particles are melt blended using a twin screw extruder. Subsequently, extraction of the continuous PEO and mineral salts using water as a selective solvent yields a highly porous PCL scaffold with fully interconnected pores. Since, the salt particles and the co-continuous polymer blend morphology lead to very different pore sizes, a particular feature of this technique is the creation of a bimodal pore size distribution. Scanning electron microscopy, mercury intrusion porosimetry and laser diffraction particle size analysis were carried out to characterize the pore morphology. The prepared scaffolds have relatively homogeneous pore structure throughout the matrix and the porosity can be controlled between 75% and about 88% by altering the initial volume fraction of salt particles and to a lesser extent by changing the PCL/PEO composition ratio. Compared to the conventional salt leaching technique and to its different variants, the proposed process allows a better interconnection between the large pores left by the salt leaching and a fully interconnected porous structure resulting from the selective polymer leaching. The average compressive modulus of the different porous scaffolds was found to decrease from 5.2 MPa to about 1 MPa with increasing porosity, according to a power–law relationship. Since, the blending and molding of the scaffold (prior to leaching) can be made using conventional polymer processing equipment, this process seems very promising for a large scale production of porous scaffold of many sizes and in an economic way.

Crown Copyright © 2006 Published by Elsevier Ltd. All rights reserved.

*Keywords:* Polymer blends; Particulate leaching; Porous scaffolds

## 1. Introduction

In the last few decades, cell transplantation using a highly porous artificial extracellular matrix, or scaffold, as supporting material has been explored as a route to repair damaged tissues. Indeed, it is known that isolated cells cannot form new tissues by themselves. Rather, they need a specific environment to guide their growth and allow tissue regeneration in three-dimensions. Ideally, the polymeric material should be biocompatible, biodegradable and bioresorbable with a controlled degradation rate to match tissue ingrowth. Surprisingly, the success of such therapy greatly depends on the microstructure and the morphology of the porous structure, which is governed by the fabrication method. The regeneration

of specific tissues aided by synthetic materials mostly depends on the porosity (void volume fraction), pore size, pore shape, pore distribution (interconnection between the pores), architecture (overall shape of the object), as well as to the mechanical properties of the scaffolds. In general, a high porosity and a high interconnectivity between the pores are necessary to allow cell growth and flow transport of nutrients and metabolic waste. Thus, beside the choice of the suitable material, the first stage of tissue engineering begins with the fabrication of a porous three-dimensional scaffold.

A number of processing techniques based on textile technologies, particulate leaching, phase separation process, gas foaming, particle aggregation and solid freeform fabrication have already been developed with more or less success to produce porous biodegradable polymeric scaffolds for tissue engineering applications [1–3]. Some of the first scaffolds used to demonstrate the feasibility of tissue regeneration involved the use of non-woven fibers in the form of tassels and felts

\* Corresponding author. Tel.: +1 450 641 5201; fax: +1 450 641 5105.

E-mail address: [joel.reignier@cnrc-nrc.gc.ca](mailto:joel.reignier@cnrc-nrc.gc.ca) (J. Reignier).

consisting in individual fibers placed into a three-dimensional pattern [4–6]. A second family of techniques involves phase separation processes (liquid–liquid or solid–liquid) of polymer/solvent mixture. These techniques have been explored to produce scaffolds with porosity up to 95% [7–10]. Basically, the polymer is dissolved in a solvent and a phase separation is induced by lowering the solution temperature or adding a non-solvent to the solution. In practice this method is so sensitive to process variations that precise control of scaffold morphology is difficult. For this reason, these techniques do not lend well to reproducible production of scaffolds. The presence of polymer solvent or non-solvent residual in the scaffolds can also represent an additional limitation of phase separation techniques.

Foaming is another path to the fabrication of porous polymer scaffolds. It was carried out by dissolving a gas at elevated pressure (physical blowing agent) [11–13] or by incorporated a chemical that yields gaseous decomposition products (chemical blowing agent) [14–16]. The foaming technique generally leads to pore structures that are not as fully interconnected as the previously mentioned ones. Another feature is the ‘skin–core’ structure where the core is porous while the external skin of the sample is solid. In some cases, the resulting scaffolds can have well interconnected macroporous structure with limited core/skin effect [15]. Other techniques include the use of particle aggregation to create macroporous three-dimensional structures with porosity up to 35% [17–19] and solid freeform fabrication technique (SFF) such as 3D-printing [20], selective laser sintering [21], 3D-plotting [22], fused deposition modeling [2,23]. These techniques are time consuming and are limited to pore sizes greater than 50  $\mu\text{m}$  and to porosity lower than 70%.

One of the most common and straightforward technique to prepare porous scaffolds is the particulate leaching method, which involves the selective leaching of a mineral, usually NaCl salt or of an organic compound such as saccharose to generate the pores. Solvent casting/particulate leaching involves the casting of a polymer solution and dispersed calibrated porogen particulates in a mold, removal of the polymer solvent, followed by leaching out of the porogen [24,25]. Because of casting and solvent evaporation step, this technique is suitable for thin scaffolds only. One drawback in this technique is the presence of organic solvent, which may be hard to completely remove from the scaffolds during the drying process. Residual organic solvent may be harmful to adherent cells or nearby tissues. To circumvent this problem, several authors proposed to replace solvent casting by melt-molding resulting in the melt-molding/particulate leaching method. Briefly, the melt-molding step consists in premixing polymer powder and solid porogen particulates and hot-pressing them together. The samples are then subjected to the same solid porogen leaching step as for the solvent-cast samples [26–29]. In a general manner, the major advantage of particulate leaching methods is the effective control of porosity and pore size. Materials with porosity levels up to 90% and pore size varying between 100 and 700  $\mu\text{m}$  have been reported using the particulate leaching technique. The porosity (or void volume

fraction) is given by the amount of leachable particles, whereas the pore size and pore shape of the porous structure can be modified independently of the porosity by varying the leachable particles characteristics (size and shape). One potential deficiency of the technique, especially for scaffolds requiring lower porosity levels is the lack of interconnectivity between the pores. Indeed, the spatial organization of the porous structure—including the interconnectivity between the pores—is directly dictated by the spatial arrangement of the porogen particles in the polymer/particulate composite. Therefore, decreasing the volume fraction of porogen particles decreases the number of contact point between particles and thus decreases interconnection between the pores after leaching of the porogen particles. Thus, it can lead to the entrapment in the polymer matrix of porogen particles that are not in direct contact with other particles. This phenomenon is particularly important at low volume fraction of porogen particles, typically less than 65% for rigid spheres. In that case, a completely open-cell structure cannot be manufactured due to the isolated particles in the polymer matrix [24,29]. Another feature that is noteworthy for the scaffold application is that the interconnection between the pores is smaller than the size of the pores. This may limit the propagation of cells from one pore to the other in certain applications. Therefore, even if the pore interconnection can be obtained using high porogen volume fraction, it cannot accurately be controlled. Recognizing this limitation, it has been proposed to partially bond the porogen particles by working in a humid environment in the case of NaCl porogen or by heat treatment in the case of paraffin spheres or sugar particles [24,30,31].

To improve the interconnectivity between the pores, other novel scaffolds preparation methods have been proposed by combining particulate leaching with other fabrication techniques, such as phase separation, emulsion freeze-drying, gas foaming or rapid prototyping [13,32–36]. However, combination of particulate leaching with phase separation technique or combination with gas foaming techniques does not ensure complete interconnectivity of the porous structure. Rather, it results in the creation of a multi-porous structure characterized by different pore sizes and/or pore morphologies, the larger pores typically resulting from the extraction of the porogen particles whereas the smaller pores are characteristic of the combinatory method. In another approach, solvent casting/particulate leaching was coupled with solid freeform manufacturing. This lead to scaffolds containing huge channels created by the computer aided system dispersed in small randomly distributed local pores generated by leaching of porogen particles [34]. In spite of the increase in porosity due to addition of porogen particles, none of these methods allowed a complete control over the interconnected pore structure.

More recently, a new methodology for the preparation of porous scaffolds for tissue engineering has emerged from the melt blending of two immiscible polymers [37,38]. The strategy used consists in melt blending the two polymers in the judicious composition required to create the so-called co-continuous blend morphology, an interconnected structure in which each phase is fully continuous. At dispersed phase

content beyond the percolation point ( $\cong 15$  vol%), the minor phase starts to form elongated structures that can touch to create an interconnected network. The full continuity of both immiscible phases however, is only possible in the concentration range close to the phase inversion point. Clearly, at that point, it is not possible to distinguish between a matrix and a dispersed phase. This co-continuous morphology generally occurs in the 40:60–60:40 (vol%) composition range. After melt mixing, the size scale of the blend is generally in the order of 1–10  $\mu\text{m}$  but can be greatly increased to 100–200  $\mu\text{m}$  by annealing above the melting temperature (semi-crystalline polymer) or glass transition temperature (amorphous polymer) of the two components. Subsequently, complete extraction of one of the polymer phases using a selective solvent is possible due to the full continuity of the two phases. The leaching, therefore, leads to a porous structure with fully interconnected pores. It is noteworthy that in the scaffolds prepared by polymer leaching, the pore structure is characterized by the interconnection of cylinders and thus is completely different than those observed with the others techniques where the larger pores are generally interconnected through smaller gates. Due to that specific pore network structure, the polymer leached scaffolds are particularly suitable for load bearing applications such as bone or cartilage regeneration. Another important advantage from a manufacturing point of view is that melt processing techniques such as extrusion and injection molding can be used to make porous scaffolds with complex geometries in an economic way. One drawback of the technique is that it yields maximum porosity of 50–60%. To increase this limit, the polymer leaching technique will be combined in the current study with a particulate leaching technique. In order to maintain the advantages related to melt processing techniques, the particulate loading will be kept in a range where the material can still flow in the molten state.

The purpose of this study is to evaluate the feasibility of a preparation method combining polymer and particulate leaching techniques for the preparation of highly interconnected three-dimensional polymeric porous scaffolds. More specifically, sodium chloride salt and polyethylene oxide will be used as water soluble porogens to form porous polycaprolactone scaffolds. The polycaprolactone and polyethylene oxide are known to be immiscible and, therefore, form a fully phase-segregated blend [39]. The maximum amount of salt particles that can be added to the polymer blend while keeping flow conditions will first be determined. Then, a detailed study of the pore size and NaCl particle size will be addressed to measure the influence of the intensive mixing which is

generated inside the extruder on the integrity of salt particles. The results will be correlated with the morphology of the porous samples observed by scanning electron microscopy.

## 2. Experimental

### 2.1. Materials

Poly( $\epsilon$ -caprolactone) (PCL tone P-787) and polyethylene oxide (PEO WSR N-10) were obtained from Dow Chemicals. Some of their characteristics are reported in Table 1. Analytical grade chloroform was purchased from Aldrich Chemical Co. Ltd. Table salt was used as the particulate porogen. The salt was dried under vacuum at 100 °C prior to blending. The PCL and PEO were received in sealed containers that minimize moisture absorption and were further dried at 50 °C under vacuum for a minimum of 24 h prior to extrusion.

Rheological characterization of the different polymers was carried out by oscillatory shear rheometry using a Rheometric Scientific rheometer (Ares). The experiments were performed in parallel-plate geometry with a gap of 1.2 mm at a temperature of 100 °C and under a nitrogen atmosphere to avoid degradation of the polymers. The dynamic mode was used to measure the complex viscosity ( $\eta^*$ ) as a function of frequency. The stability of the neat materials at 100 °C was monitored for 5 h using an oscillation frequency of 0.1 Hz. All the measurements were performed at low strain amplitudes (about 0.5–1%). The complex viscosity of the neat materials at 100 °C is shown in Fig. 1 as a function of frequency. At low frequency, the PCL is characterized by a well defined Newtonian plateau. The PEO is more shear-thinning in the probed frequency range. The PEO is less viscous at low frequency but the viscosity curves cross each other at around 20  $\text{s}^{-1}$  and at this point, the PEO becomes the most viscous component. The PCL/PEO viscosity ratio is around 3.8 at 100  $\text{s}^{-1}$ .

### 2.2. Preparation of porous PCL

The compounding of polymers and salt particles was carried out on a 30 mm twin-screw extruder (ZSK-30) operating at 100 °C and at a rotation speed of 150 rpm. The salt particles and the polymers were added together in the primary feed port. The screw configuration, reported on Fig. 2, was specially designed to minimize shear and viscous heating in the highly filled compounds that are produced. It is noteworthy that no reverse screw elements, typically used to build pressurized

Table 1  
Characteristics of the pure materials used in this study

Materials	$M_n \times 10^{-3}$ (g/mol) <sup>a</sup>	$T_g$ (°C) <sup>a</sup>	$T_m$ (°C) <sup>a</sup>	Melt flow index (g/10 min) <sup>a</sup>	Density (g/cm <sup>3</sup> ) <sup>b</sup> at	
					23 °C	100 °C
PCL	$\cong 80$	–69	60	0.5	1.14	1.036
PEO	$\cong 100$	–70	65	–	1.21	1.07
NaCl	n/a	n/a	801	n/a	2.17	–

<sup>a</sup> Obtained from suppliers.

<sup>b</sup> Estimated from PVT equations.

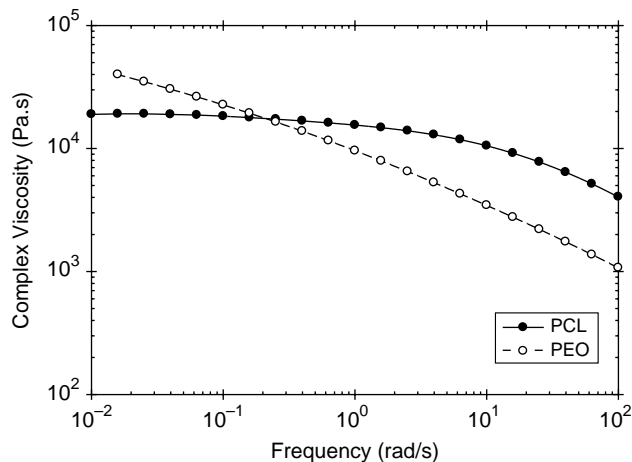


Fig. 1. Complex viscosity of pure PCL (black symbol) and PEO (white symbol) at 100 °C as a function of frequency.

areas in the twin-screw extruder, were used in the configuration. In addition, a non-restrictive extrusion die was used to minimize the pressure buildup at the end of the screw. The resulting polymer/salt composites were cut from the exit of the extruder and dropped directly into a bath of liquid nitrogen, in order to freeze in the morphology. Different polymer-salt compositions were used. In a first approach, the PCL/PEO composition ratio was kept constant at 50/50 to ensure a co-continuous morphology of the polymer components while changing the concentration of NaCl. In a second part, the PCL/PEO composition ratio was decreased to maximize porosity of the scaffold while keeping the mechanical integrity of the samples. In both cases, the resulting polymer/salt composites were immersed in deionized water to leach out the salt and PEO. The water was changed every 12 h up to a constant weight of the wet sample was obtained.

### 2.3. Morphology observation

A scanning electron microscope (SEM), Hitachi SR-4700, operated at 1 kV voltage, was used to examine the scaffold morphology. The PCL/PEO/NaCl composites were fractured in liquid nitrogen and etched with deionized water for 48 h at ambient temperature to selectively extract the water soluble

components (PEO and NaCl salt particles). The cross-sections were coated with platinum using a sputter coater (Emitech K575X) operating at 10 mA for about 15 s under argon atmosphere.

### 2.4. Solvent extraction and continuity of the PEO phase

Selective solvent extractions of PEO in deionized water were performed for one week at room temperature over the whole composition range in order to determine the phase inversion point for the PCL/PEO system. Weight-loss measurements were carried out to evaluate the extent of continuity of PEO using the following equation:

$$\% \text{ Continuity} = \left( \frac{\text{weight PEO}_{\text{initial}} - \text{weight PEO}_{\text{final}}}{\text{weight PEO}_{\text{initial}}} \right) \times 100 \quad (1)$$

The maximum error is estimated at  $\pm 2\%$  continuity units.

### 2.5. Porosity measurement

Assuming that both porogen agents are completely extracted out due to the co-continuous morphology of the PCL/PEO blends (see 3.4 for a demonstration), the porosity or void volume fraction  $V_f$  (%) of the PCL scaffolds was calculated using the following equation

$$V_f = \left( 1 - \frac{\rho^*}{\rho_s} \right) \times 100 \quad (2)$$

where  $\rho^*$  is the apparent density of the porous scaffold and  $\rho_s$  is the density of the non-porous material.

For comparison purpose, porosity measurements were also investigated on PCL/NaCl binary blends. In that case, the porosity was calculated using the following equation

$$V_f = \frac{(\rho_s - \rho^*)}{\rho_{\text{NaCl}}} \times 100 \quad (3)$$

where  $\rho_{\text{NaCl}}$  is the density of salt (Table 1). This calculation allows us to take into account of the possible incomplete dissolution of the salt crystals. Note that in both cases the estimation of porosity is done on disk shaped samples with

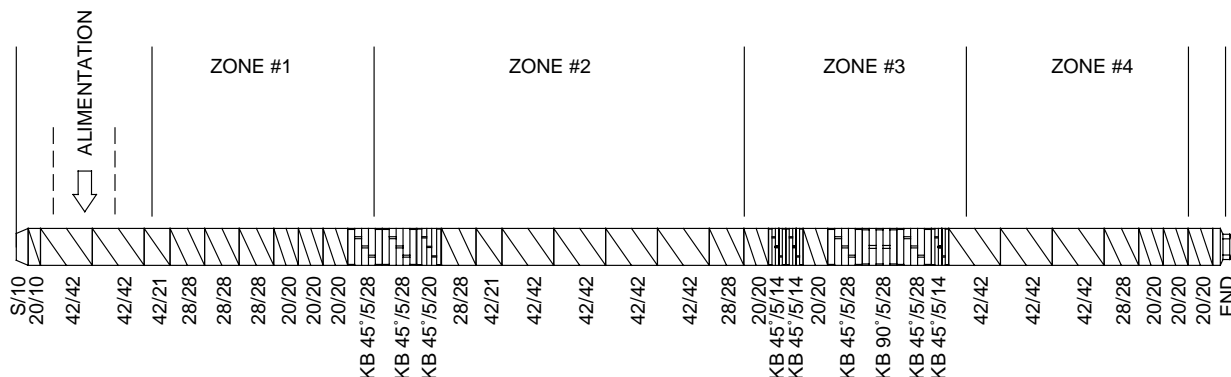


Fig. 2. Schematic of screw configuration in the twin-screws compounding process. The screw have a 30 mm diameter. The gap between the screw tip and the barrel is 0.4 mm.

slight irregularities on the plane surface due to the cutting stage.

### 2.6. Mercury intrusion porosimetry

A Micromeritics Poresizer 9320 was used to determine pore size distribution and pore volume of the PCL scaffolds. This technique is based on the non-wetting behavior of mercury with respect to most solids, which then opposes its entrance into the porous structure. After evacuation of all the gas from the volume containing the samples, mercury is introduced into the sample container and then forced into the pores by applying an external pressure. The direct relationship between this pressure and the intruded volume of mercury is provided by the Washburn equation

$$\Delta P = \frac{2\sigma \cos \theta}{R} \quad (4)$$

where  $\Delta P$  is the applied pressure,  $R$  is the pore radius,  $\sigma$  the surface tension and  $\theta$  is the contact angle. A mercury contact angle of  $140^\circ$  and an interfacial tension of mercury of  $485 \text{ mN/m}$  were used. This technique allows to investigate pore size in the range of a few tens of nanometre to about  $500 \mu\text{m}$ .

### 2.7. NaCl particle size

The size distribution of NaCl particles was estimated using a Beckman Coulter laser diffraction particle size analyzer (model LS 13 320). This single wavelength system counts and sizes particles in powder form with a size range from  $0.4$  to  $2000 \mu\text{m}$ . The PCL/PEO/NaCl composites were plunged into chloroform to selectively extract both polymers. The polymer solution was changed several times until a clear solution was obtained. The NaCl crystals were then collected and dried under vacuum for 24 h before analysis.

### 2.8. NaCl residues

The concentration of NaCl residues into the PCL porous scaffolds, i.e. after dissolution of the two porogen agents, was estimated by measurement of the chlorides. The following procedure was used. The PCL scaffolds were washed several times in deionized water until the water was free of chloride. This step is essential to ensure a complete dissolution of the NaCl, which is not entrapped into the PCL phase. Then the samples were plunged into chloroform, which only dissolves the polymers but not the NaCl residues. The NaCl residues were then extracted in deionized water five times to obtain a  $100 \text{ mL}$  solution, which was further analyzed using a calibrated electrode. The measurement of the voltage allows determining chloride concentrations as low as  $10^{-2} \text{ ppm}$ .

### 2.9. Mechanical properties

Compressive properties were carried out on an Instron testing machine (model 5500R) with a  $1 \text{ kN}$  load cell. Tensile

test were performed on cylindrical samples ( $6 \text{ mm}$  in diameter and  $3.7 \text{ mm}$  thick) directly punched in a porous PCL sheet. The crosshead speed was kept at a value of  $1 \text{ mm min}^{-1}$ . The reported values are the average of five tests for each sample composition. All these tests were carried out at ambient temperature ( $23^\circ\text{C}$ ). The compressive modulus was evaluated from the entire linear elastic region of the stress–strain curve.

## 3. Results and discussion

### 3.1. Co-continuous blend morphologies

The co-continuous blend morphology can be found in a concentration range that depends on the viscosity ratio between the polymeric blend components. The vast majority of the theoretical models for the prediction of phase inversion point assume that the phase morphology of binary polymer blends is a function of the viscosity ratio between the blend components. In all cases, a viscosity ratio equal to 1 leads to a phase inversion point at the 50:50 composition. When the two components have different viscosity, the less viscous component tends to encapsulate the more viscous one thus pushing the phase inversion point toward a blend that is richer in the most viscous component. In our study, the viscosity differences between the blend components are relatively modest and a phase inversion point close to the 50/50 (%vol) may be expected.

In the current fabrication technique, the PEO phase has to be extracted out in order to yield the desired porous PCL structure. It is, therefore, important to determine the concentration range in which the PEO phase can be assumed continuous. In turn, this concentration will correspond to the potential porosity level that can be reached after leaching. As a first step, the relation between the composition of the blend and the degree of continuity of the PEO phase has been explored for the binary polymer blend (i.e. without the NaCl salt particles) and is given in Fig. 3. The full continuity of the PEO phase is reached at

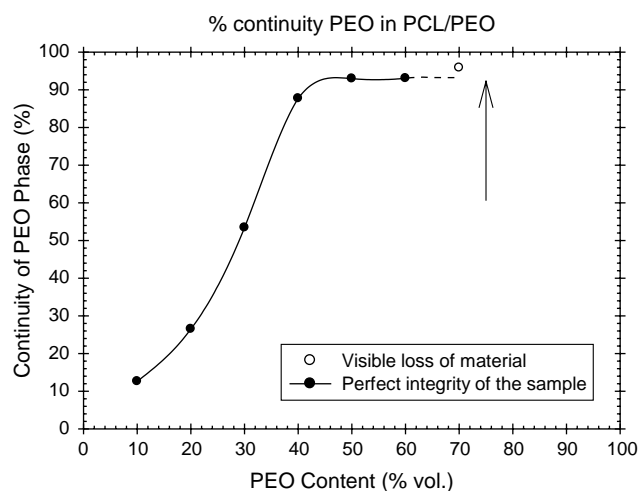


Fig. 3. PEO phase continuity as a function of PEO content. The white circle indicates the concentration at which visible loss of material appears. A black arrow indicates the onset point of disintegration of the samples.

a concentration slightly higher than 40% PEO. This represents the lower PEO concentration limit required for complete removal of the PEO during the leaching step. The higher concentration limit will be given by the point when the PCL scaffold loses its integrity corresponding to the continuous to dispersed morphology transition of the PCL phase. Further increase of the PEO concentration was possible up to about 70 vol% PEO while keeping the mechanical integrity of the sample. At this point, the samples began to show visible loss of material (white circle in Fig. 3) during extraction due to surface erosion. Further increase of the PEO concentration beyond 70% led to the complete disintegration of the sample into a powder (as indicated by a black arrow in Fig. 3), indicating that phase inversion occurred and thus the PCL became the dispersed phase.

### 3.2. PCL scaffold morphology

The morphology obtained in absence of the salt particulates was first explored. In this case, the pore size obtained using the polymer leaching technique is dictated solely by the scale of segregation in the co-continuous polymer blend. To determine this pore size, microtomed surfaces of 50/50 PCL/PEO blends have been observed by SEM after extraction of the PEO phase, as illustrated in Fig. 4. As expected from the gravimetric results, the PCL porous scaffold possesses fully interconnected pores. The presence of PEO subinclusions into the PCL phase—clearly visible in Fig. 4(b)—could possibly explain that the plateau value in gravimetric curve is lower than 100%. A few authors reported the presence of subinclusions in binary blends such as PLLA/PS [38]. Even if it is not the purpose of this work to discuss the issue of subinclusion formation in co-continuous blend morphology, their presence into the PCL phase even in small amount is of critical interest since it implies that part of the porogen will not be extracted out, rather staying into the PCL phase as dispersed droplets of submicron size. It is, therefore, important when using this technique to use a porogen phase that is biocompatible (such as PEO).

With the addition of salt particulates, the scaffold porosity can be tuned by modifying the salt concentration giving an additional degree of freedom in the scaffold design. In this case, an immediate concern which arises has to be the maximum salt concentration that can be attained while maintaining sufficient fluidity for processing the material in extrusion or injection molding equipments. The viscosity of suspensions is known to increase with solid particulate concentration and to become infinite when the solid content reaches the maximum packing concentration [40]. The maximum packing for monodisperse dense sphere is theoretically around 68 vol%. At that point, particles contact each other and there is no longer sufficient liquid phase to lubricate the motion of particles. In our case, starting from 10% with step of 10%, the maximum salt concentration that was attained was 70 vol% and thus was in the range of the expected maximum packing concentration. Beyond that concentration, the particulates were not totally wetted and the mixture lost its ability to flow condition. The SEM micrographs shown in Fig. 5 illustrate the morphology of

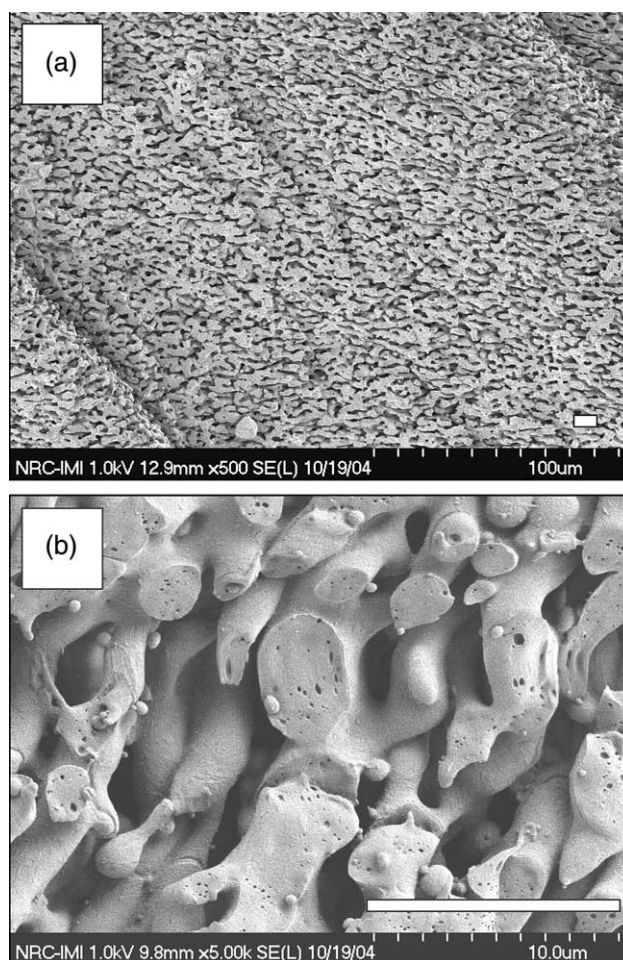


Fig. 4. SEM photomicrographs at two different magnifications of the surface of PCL/PEO 50/50 (%vol) sample after dissolution of the PEO phase. The white bar denotes 10 µm in both images. The presence of small droplets of PEO, which are entrapped inside the PCL phase is clearly shown in part (b).

the PCL porous scaffolds for NaCl concentration of 50, 60 and 70%. Note that in all cases the PCL/PEO concentration ratio is kept constant to 50:50. The nominal porosity level expected for the 50, 60 and 70 vol% salt blends is thus 75, 80 and 85%. From a macroscopic point of view, the morphological structure does not change significantly with NaCl composition varying from 50 to 70% (Fig. 5(a), (c) and (e)). All scaffolds are characterized by a multimodal pore structure with distinct pore sizes and pore architectures. The macropores associated with the salt particles are roughly cubic in shape and seems to be homogeneously distributed in the melt polymer matrix. These macropores are most easily seen at low magnification and at the 50 and 60 vol% salt levels (Fig. 5(a) and (c)) where the rectangular pores span over several hundred µm. The size of these macropores varies considerably throughout the scaffold from a few tens to hundreds of micrometers and should depend on the size distribution of the salt particles. The surface of the macropores—corresponding to the surface of the NaCl salt particles—demonstrates good pore interconnection with the porous matrix, indicating that no particular skin layer was formed on the surface of the salt particle (Fig. 5(b), (d) and (f)).

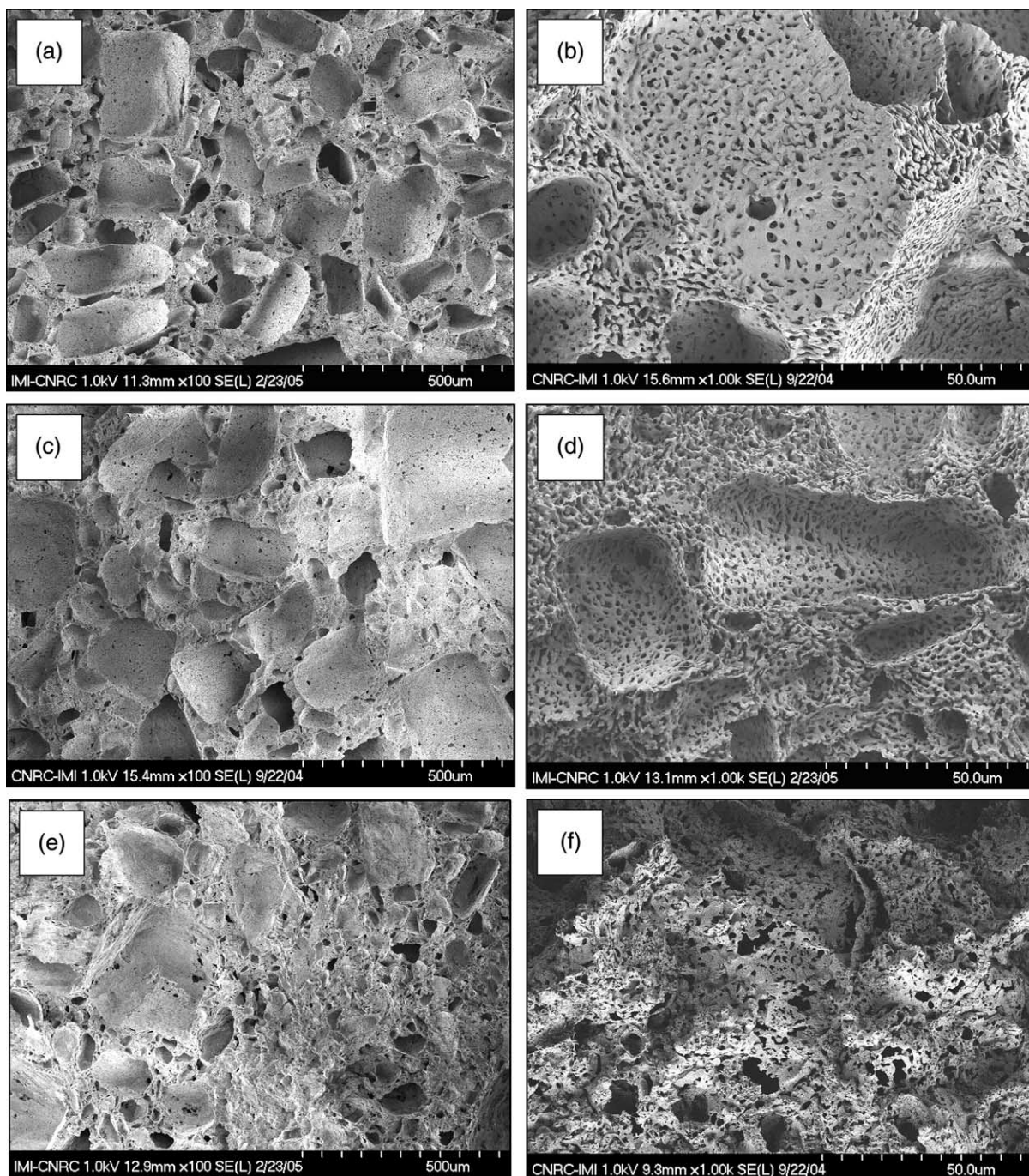


Fig. 5. SEM photomicrographs of PCL porous scaffolds generated after selective extraction of (a) and (b) 50% NaCl; (c) and (d) 60% NaCl; (e) and (f) 70% NaCl after dissolution of PEO and NaCl. In all blends the PCL/PEO composition ratio is kept constant to 50/50.

Also, the absence of remaining salt crystals suggests that the dissolution of the salt crystals is completed and that the pores are well interconnected. The micropore network created by the extraction of the PEO porogen polymer is characterized by cylindrical pores with a maximum size of approximately  $5\ \mu\text{m}$ , as shown in Fig. 6(a). On the other hand, inspection of the SEM micrographs also reveals the presence of pores of intermediate size, which may be created by contact between salt particles before leaching. Occasionally found in the 50% salt scaffold, the number of these intermediate size pores increases with salt

concentration as expected from the higher contact probability between salt particles. The size of these pores, much smaller than the size of the macropores, is typically in the  $5\text{--}50\ \mu\text{m}$  range. Compared with commonly used particulate leaching methods, the current scaffold fabrication process allows for a better connectivity between the pores since the cell walls—between the NaCl salt particles—are themselves porous (due to the removal of the continuous PEO phase). As a result, the porosity is entirely interconnected throughout the whole scaffold, even at low salt concentration. This was confirmed

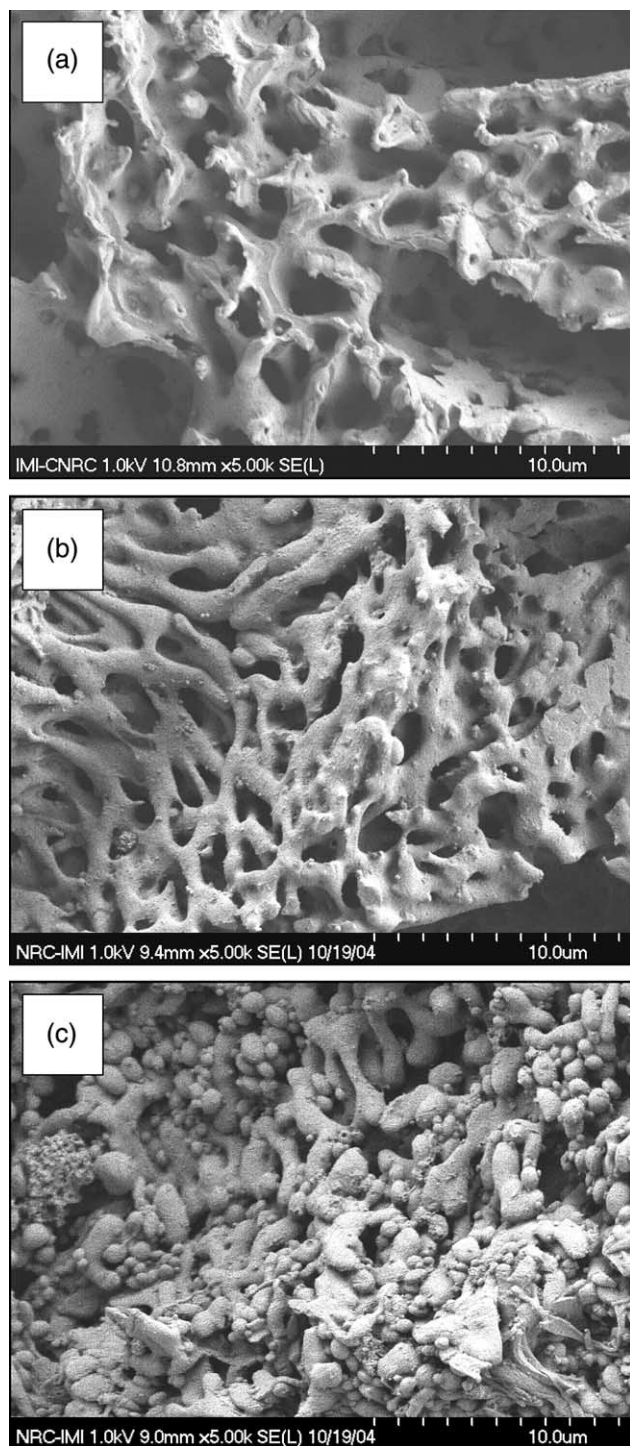


Fig. 6. SEM photomicrographs of PCL porous scaffolds after selective extraction of PEO and NaCl. The PCL/PEO composition ratio is changed while keeping the NaCl concentration at 50 vol%. (a) PCL/PEO = 50/50; (b) PCL/PEO = 40/60; (c) PCL/PEO = 30/70.

by similar morphological results obtained at lower salt concentrations.

A few comments can be made on the pore morphology with respect to the tissue engineering application. It clearly appears that the prepared scaffolds possess a very good interconnectivity between the pores, and that is strongly desired in tissue engineering, as the exchange of nutrients and cell waste would

be improved. However, it may be desirable to increase the size of the pore opening due to the extraction of the PEO phase in order to improve the cell seeding throughout the whole sample and not only on its surface. This issue has already been discussed for more than 20 years in polymer blends (without filler of macroscopic size) and it appears that the segregation scale in co-continuous blends mostly depends on the interfacial tension between the two phases. Unfortunately, in our case, there is a good affinity between the PCL and PEO phase, resulting in a low interfacial tension [39] and thus in fairly small pores. As mentioned in the introduction, the phase size in co-continuous blends can be increased by annealing the blend above the melting temperature of the two components [37,38]. In the current ternary blend however, the effect of the high salt content on the coarsening of the structure must be assessed. In comparing Figs. 4(b) and 6(a) (same magnification), it is clearly seen that the size of the micropores given by PEO leaching are significantly smaller in the presence of NaCl particles. A possible explanation is that the elapsed time before the sample was cooled below the crystallization temperature after extrusion (around 5–10 s) is sufficient to initiate the coarsening of the co-continuous PCL/PEO structure in absence of NaCl particles. This coarsening process may be slowed down or even prevented in a constrained geometry as the flow of the polymer is hindered by the presence of rigid particles. This would result in the blends comprising the NaCl particles in lower phase size as noted above. Similar changes in coarsening dynamics were observed in different polymer/polymer/particulate blends. For example, addition of a small amount of fillers (typically, 3 wt%) such as nano-clays, carbon black and calcium carbonate prevented the de-mixing or coalescence of the PS/PMMA polymer blend in presence of carbon dioxide [41]. In another investigation, the addition of black carbon in PE/PS blends—selectively localized into the PE phase—increases the stability of the co-continuous morphology during thermal treatment [42]. These authors explained the reduction in the coarsening rate during annealing by the viscosity increase in the filled-PE phase. In the current study, the size of the NaCl particles is much larger than those reported in these studies with respect to the size of the polymer phases. However, the particulate concentration is much higher possibly resulting in similar confinement effects, which could explain the increased stability of the PCL/PEO co-continuous structure. It has also been reported that adsorption of polymer chains on filler surfaces can lead to the reduction of the average segmental mobility of those chains and can thus shift a portion of the polymer relaxation spectrum to longer times, just as entanglements, partial cross-linking or crystallization do to a lesser degree [43]. As a result, this adsorption phenomenon may tend to slow down the mechanisms of coarsening which occurs in quiescent conditions. This effect will be directly related to the strength of the interaction between the chains and the filler surface and would also contribute to slow down the coarsening phenomenon in presence of the salt particulates.

The salt concentration was modified above to change the scaffold porosity level. Another way to modify the final porosity is to change the PCL/PEO composition ratio within

the co-continuous concentration range. Samples were prepared at different composition ratios, while keeping the amount of NaCl particles at a constant value of 50%. Fig. 6(a)–(c) illustrate the evolution of the pore structure for PEO concentrations (within the total 50% polymer content) of 50, 60 and 70 vol%. As in Fig. 5, the nominal porosity of these scaffold are also 75, 80 and 85%, respectively. The co-continuous structure is clearly present in Fig. 6(a) for the PEO concentration of 50%. However, increasing the proportion of PEO phase to higher concentrations in Fig. 6(b) and (c) leads to a drastic effect on the morphology of the PCL scaffold. At the PCL/PEO concentration ratio of 40/60, the PCL phase is still continuous but the PCL phase presents a fibrillar structure. The space between the PCL struts seems to increase while the PCL phase thickness remains relatively constant. The micrograph for the 30/70 PCL/PEO blend in Fig. 6(c) shows PCL isolated nodules indicating the loss of the PCL phase continuity. This blend morphology evolution with composition ratio clearly supports the continuity-composition curve of the PEO phase presented in Fig. 3 and explains the sample fragility and surface erosion observed during porogen leaching. Samples corresponding to PCL/PEO concentration ratio of 20/80 totally collapsed during leaching (not shown), clearly indicating that phase inversion occurred and that PEO became the matrix while the PCL was only present as dispersed droplets.

### 3.3. Overall porosity

The apparent porosity associated with the micrographs of Figs. 5 and 6 are those expected from the complete removal of the polymer and salt porogen. It is very important to quantitatively verify if this assumption is realistic. To further investigate this point, final weight of the samples after drying and exact dimensions were used to evaluate the density and the porosity of the PCL scaffolds as a function of the salt concentration. Fig. 7 shows the measured porosity as a function of the porosity expected from complete removal of the porogen

fraction. For the PCL/PEO/NaCl blends, the measured porosities of the scaffolds correspond well with the predicted ones. As expected, increasing the amount of porogen and/or reducing the PCL/PEO composition ratio induced an increase in porosity. The highest porosity level, 88%, was obtained with the 12/18/70 PCL/PEO/NaCl. All these results imply that both the salt and the PEO are fully extracted, that the pores are well interconnected, and more importantly, that adding NaCl as a second porogen into PCL/PEO blends allows to greatly extend the maximum porosity value.

For comparison purpose, PCL/NaCl binary blends with the same NaCl concentrations were also prepared. As shown in Fig. 7, the porosity measurements obtained for these blends (without PEO) are lower than the values expected for complete extraction (solid line), except for the 70% salt blend concentration. These lower porosity values indicate that part of the salt crystals are entrapped into the PCL phase at low salt concentration and thus cannot be leached out with water. This phenomenon has also been observed by several authors [29] on PLGA scaffolds made by using gelatin microspheres as porogen agent. They reported that their PLGA scaffolds still contain between 3 and 9 wt% of residual gelatin—the porogen phase they used—at the end of the dissolution process, and that this fraction tended to decrease with increasing initial fraction of gelatin. Similarly, other researchers reported that it was not possible to leach out the salt component from compression molded samples at salt contents below 60% [24].

It is also noteworthy in this study that the co-continuous polymer blend structure speeds up the salt release process since it takes only 2–3 days to completely remove the NaCl from the PCL/PEO/NaCl blends compared to almost 2 weeks for the PCL/NaCl blends. The above results clearly indicate that adding a polymer phase as a second continuous porogen overcomes one of the main disadvantages of the classical salt leaching method, namely the lack of interconnection between the porogen particles, particularly at low salt concentration, which leads to incomplete extraction of the porogen phase.

### 3.4. Pore network characteristics

In this part of the work, the pore network will be examined in details by comparing the NaCl particle size and the mercury intrusion porosimetry analysis. For the particle size analysis, the NaCl particles were extracted out from the PCL/PEO/NaCl composites by selective dissolution of the polymeric materials and decantation. They were then analyzed by laser diffraction. Clearly, it would be desirable to control and maintain a specified salt particle size distribution prior to leaching, since the macropores described above are the fingerprints of the volume occupied by the NaCl particles. Thus, studying the effect of mixing on the salt particles size and shape is of critical interest. Fig. 8 depicts the particle size distribution of NaCl particles before and after mixing. The size distribution by number of particles reflects the number fraction of the particle population in different size categories. On the other side, the size distribution by volume represents the volume fraction of the particles in different size categories. Because small

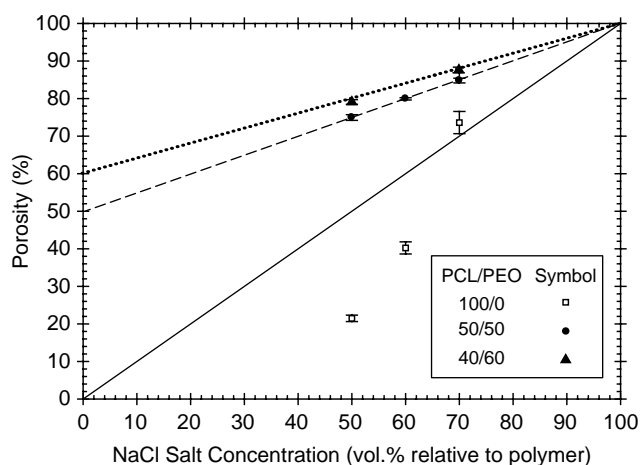


Fig. 7. Porosity of PCL scaffolds as a function of NaCl concentration. The solid, dashed and dotted lines represent the theoretical porosities that should be obtained for PCL/PEO composition of 100/0, 50/50 and 40/60, respectively, if complete extraction of porogen agents occurs.

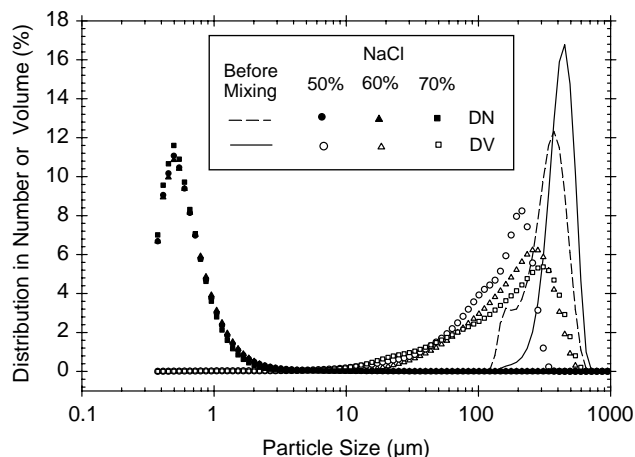


Fig. 8. Effect of mixing on the size of NaCl particles. (a) Before extrusion; (b) after extrusion, for the 25/25/50, 20/20/60 and 15/15/70 (vol%) PCL/PEO/NaCl blends. The number (DN) and volume (DV) distribution reflect, respectively, the number and volume fraction of the particle population in different size categories.

particles necessarily occupy less volume than large ones, the peak in the number distribution always occurs at a smaller size than the peak in the volume distribution (unless the particles are monodisperse). Before mixing (solid line and dashed line), the NaCl powder is mainly composed of uniformly distributed large particles—typically between 100 and 700  $\mu\text{m}$  in diameter—as demonstrated by the similar volume (DV) and number (DN) size distribution curves. However, after going through the extruder, the number and volume particle size distributions move apart, indicating that a large number of small particles appeared during mixing. The cumulative number and volume size distributions given in Table 2 indicates that the vast majority of particles—more than 80% in population—have a particle diameter smaller than 1  $\mu\text{m}$  but they represent as less as 0.2% of the total volume of NaCl particles. It is worth noting that this volume fraction may be slightly increased by the lost of the smallest particles—the lightest particles—in suspension into the solvent during extraction of the polymeric phases. However, this proportion should not significantly affect the results. Table 2 also indicates that about 70 and 90% of the volume is given by particles larger than 100 and 10  $\mu\text{m}$ , respectively. Similar distribution curves, were found using the different NaCl concentrations indicating that particle size distribution is independent of the salt concentration in the 50–70% salt range. Because of the

Table 2

Cumulative number and volume size distributions of NaCl salt particles before and after mixing for the different salt composition

Particle size ( $\mu\text{m}$ )	Cumulative% <							
	Before mixing		50% NaCl		60% NaCl		70% NaCl	
	Num%	Vol%	Num%	Vol%	Num%	Vol%	Num%	Vol%
1	0	0	86.0	0.16	86.1	0.11	88.82	0.2
10	0	0	99.8	1.6	99.9	0.67	99.85	1.6
100	3.2	0.1	99.99	30.9	99.99	22.3	99.99	29
1000	100	100	100	100	100	100	100	100

In all cases the PCL/PEO composition ratio is kept constant at 50/50.

occurrence of a huge population of small particles, the distribution in number—traditionally given in particle size analysis—does not yield a representative image of the NaCl particle size after mixing. From a processing point of view, using a relative wide range of particles sizes can decrease the viscosity of the blend for a given filler concentration compare with monodispersed systems [40]. This phenomenon simply results from the increase in the maximum packing fraction as smaller particles can occupy the space in the interstices between larger ones.

SEM micrographs of the NaCl powder before and after mixing are given in Fig. 9 to illustrate the effect of mixing on salt particles. Before mixing, the salt particles have a cubic shape with relatively sharp edges. However, after mixing, the vast majority of salt particles has been fractured in various shapes and look more round in shape. In addition, a large number of very small salt particles are present on the micrograph, as expected from the particle size analysis given in Fig. 8. All the above results demonstrate that erosion and fracture—by cleavage—are taking place during intensive mixing into the extruder. Different screw configurations or mixing equipment should be investigated in the future to solve this issue.

In the second approach, the porous structure obtained after extraction of the porogen phases was directly characterized by mercury intrusion porosimetry (MIP), which is a reliable method to determine pore size distribution. Fig. 10 shows the evolution of the pore volume—reported as an incremental intrusion volume—as a function of pore diameter or pore size, measured through an increase in the applied pressure. Note that a logarithmic pore-size axis has been chosen because it is more suitable for covering several orders of magnitude in pore size, as it is the case in our study. The most striking feature is that the majority of pore volume seems to be occupied by pores smaller than 10  $\mu\text{m}$ . More precisely, the intruded volume of pores lower than 10  $\mu\text{m}$  represents more than 57% of the overall scaffold porosity, as shown in Table 3 where the cumulative volume size distribution is given as a function of the pore size or pore diameter. According to the MIP analysis, pores greater than 100  $\mu\text{m}$  represent less than 6% of the total volume of pores whereas salt particles of equivalent sizes represent more than 70% of the total volume of NaCl particles. Clearly, this does not match the pore size distribution expected from the NaCl particle size analysis given in Table 2 where the volume of particles smaller than 10  $\mu\text{m}$  represents less than 1.6% of the total volume of particles. In addition, this discrepancy cannot

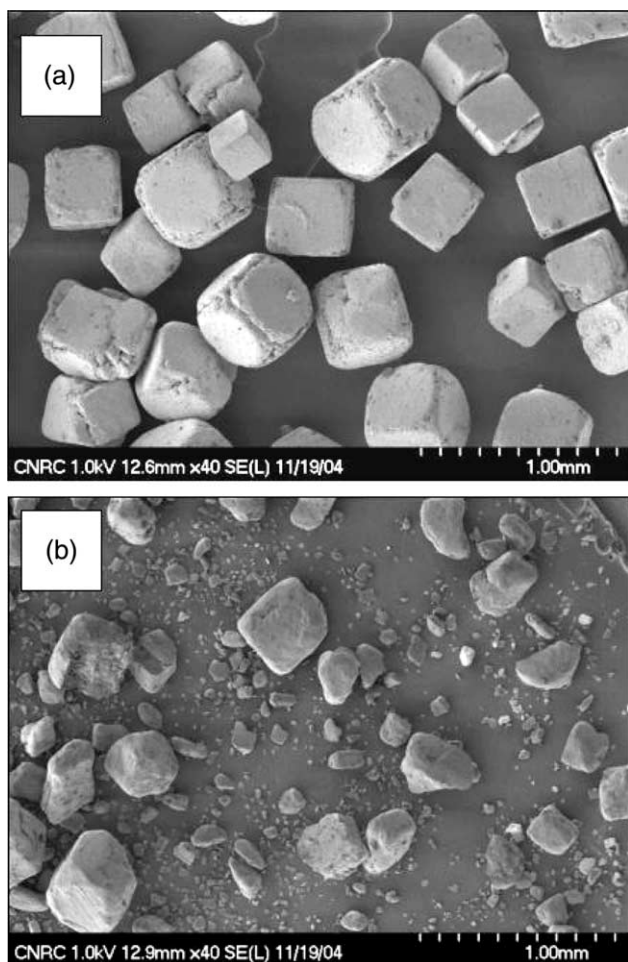


Fig. 9. SEM micrographs of NaCl particles (a) Before mixing and (b) after mixing for the PCL/PEO/NaCl 15/15/70 vol% blend (polymers selectively dissolved). Clearly, erosion and breakdown are taking place during intensive mixing into the extruder.

be only explained by the presence of the pores obtained by the polymer leaching step since the extracted PEO phase accounts only for 25% of the overall material volume (prior to leaching). How can we explain this major difference? The answer to this question lies in the implicit assumption in the MIP technique that the pore channels have uniform dimensions. In the case of non-uniform channels, the mercury intrusion will however, be influenced by presence of flow restrictions such as gates in the channels. The distribution of pore volume will, therefore, be affected by the pore opening or pore gate—gates are defined as smaller apertures linking larger diameter pores. In other words, the pore size distribution given by MIP analysis should not be understood as the volume distribution of cavities, but rather as the size distribution of the pore gates towards pores [44]. As a result, the calculated pore size distributions are always shifted towards smaller pore size [45]. As demonstrated in Fig. 5(b), the porous scaffold consists in an assembly of isolated large cavities, created by the leaching of the salt particles, interconnected by a network of smaller channels created by the PEO extraction. Given this pore structure, the results given by MIP in combination with the NaCl particle size analysis indicate that the majority of pore volume is constituted of

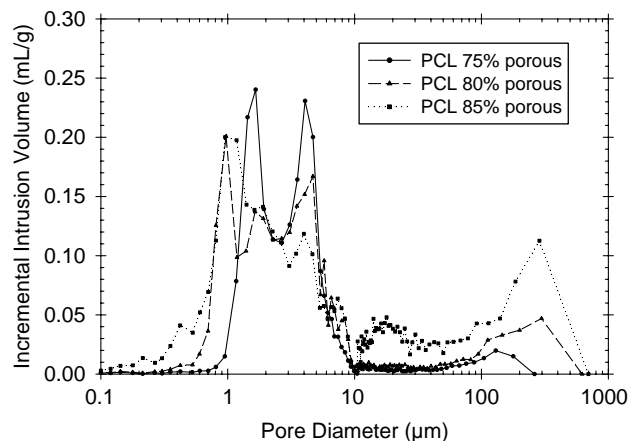


Fig. 10. Pore size distribution obtained by mercury intrusion porosimetry of the 25/25/50, 20/20/60 and 15/15/70 (vol%) PCL/PEO/NaCl blends after extraction. Data beyond a pore diameter of 300  $\mu\text{m}$  are not significant due to the low pressure reading.

relatively large pore that are only accessible through relatively small gates. As mentioned in the introduction part, this pore opening is of critical importance for cell seeding since isolated cells or cell aggregates larger than the pore opening may not be able to penetrate deeply into the scaffold.

Additional information about the difference in pore structure between the different PCL porous scaffolds can be extracted from the injection curve—the relationship of volume entering the pore system to pressure over the whole pressure range—and are given in Fig. 11. Such curves are useful in interpreting pore geometry and give information about pore to gate ratio and connectivity [46]. Firstly, the threshold injection pressure—as defined by the pressure at which there is an abrupt change of gradient in the initial part of the injection curve—decreases with porosity, and this effect is more pronounced for the higher porosity sample. Assuming a cylindrical gate size, the threshold pressures correspond to an equivalent gate size of 7, 11 and 36  $\mu\text{m}$  for the 75, 80 and 85% porous scaffold, respectively. Another important feature of Fig. 11 is the slope of the mercury capillary pressure curves for small increment above the threshold pressure. Clearly, the injection curve for the 85% porous system has a steeper gradient, which indicates that this sample has a wider range of gate sizes. All these results demonstrate that the pore structure of the 85% porous system—corresponding to the highest content of NaCl (70%)—is different from the two lower porous systems. Such a high threshold pore size—far greater than the pore size given solely by extraction of the PEO phase

Table 3  
Cumulative volume size distributions of pores for the different salt composition

Pore size ( $\mu\text{m}$ )	Cumulative volume% <		
	50% NaCl	60% NaCl	70% NaCl
1	1.3	7.8	13
10	89.7	82.0	57.1
100	97.8	94.3	92.8
1000	100	100	100

The PCL/PEO composition ratio is kept constant at 50/50.

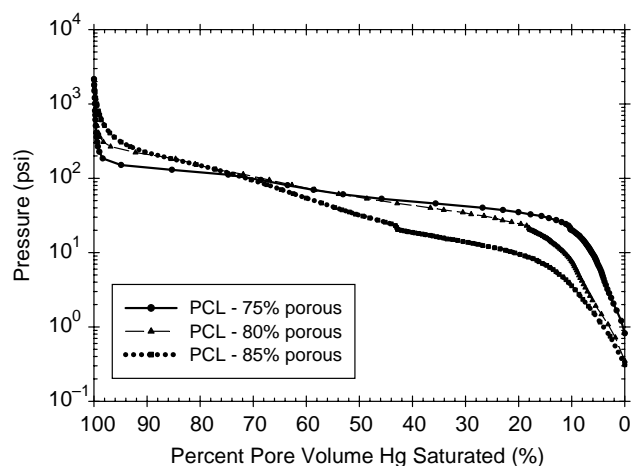


Fig. 11. Pressure–volume injection curve for PCL porous samples. Pore size distribution obtained by mercury intrusion porosimetry of the 25/25/50, 20/20/60 and 15/15/70 (vol%) PCL/PEO/NaCl blends after porogen extraction.

(<5  $\mu\text{m}$ )—as well as a steeper gradient indicate that a network of intermediate pore sizes has been created by contact between NaCl salt particles. As expected, this effect is more pronounced for higher NaCl salt content in the composite since the probability of interparticle contact should also increase in consequence (compare Fig. 5(b) and (f)). This is confirmed by estimation (from Table 3) of the relative proportion of pore gates inferred from MIP measurements between 10 and 100  $\mu\text{m}$ . With less than 10% of total pore volume for the 50 and 60% NaCl systems, this amount increases up to 35% for the 70% NaCl system. This situation is schematically represented in Fig. 12. At low salt concentrations, the particles are mainly isolated in the porous matrix (Fig. 12(a)). Thus, the interconnection between the macropores only depends on the size of the co-continuous network. However, near the maximum random packing density which is typically 64 vol% for monodispersed rigid spheres, most of the salt particles are in contact together, thus creating a second network of pore interconnection of higher sizes compared with the size of the PEO phase. This phenomena may also be accentuated by erosion of salt particles during mixing, thus increasing the surface of contact between adjacent particles. It is worth noting that an increase in volume fraction for pore size greater than 10  $\mu\text{m}$ —observed for the 70% NaCl system—may be caused to a certain extent by partial collapsing of the porous structure during mercury intrusion. Indeed, increasing the relative amount of NaCl in the blends results to thinner walls and thus one could envisage that the porous sample may be fragile enough to rupture at this weaker spots. These conditions may lead to higher apparent pore size than expected.

### 3.5. NaCl residues in the scaffold

NaCl particle size analysis clearly indicates that a large number of salt particles are in the 1  $\mu\text{m}$  size range, similar to the PEO/PCL segregation scale. Therefore, a potential concern is that the smaller salt particles may get entrapped into the PCL phase and cannot be extracted out, thus remaining inside the

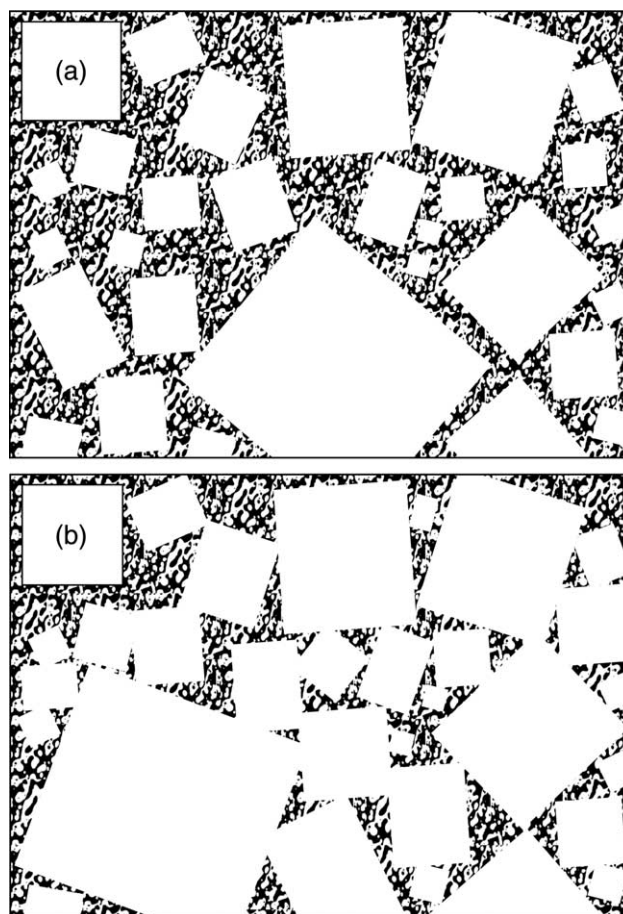


Fig. 12. Schematic representation of the effect of NaCl concentration on the pore morphology. (a) At low salt concentration, the macropores generated by salt leaching are only connected by the micropore network associated with the co-continuous PCL/PEO blend. (b) At high salt concentration, those macropores are connected by the same micropore network but also by pore opening of intermediate size due to contact between salt particles.

porous scaffold. To investigate this issue, the concentration of NaCl residues into the PCL porous scaffold with respect to the mass of the PCL scaffold after extraction were measured and are reported in Table 4. In all cases, the concentration of residual NaCl is less than 20 ppm, which represents less than 0.0005 wt% with respect to the total mass of salt particles added to the blend. Thus, even though around 0.2% volume of particles had a diameter smaller than 1  $\mu\text{m}$ , these are still fully extractable during the leaching step. It can be assumed that the particles are not completely engulfed by the PCL phase, rather protruding through the surface or even preferentially located into the PEO phase.

### 3.6. Blend morphology formation mechanism

The information presented in the previous sections enables discussion of the pore formation mechanism. One first important observation is that the co-continuity of the melt phases can be achieved regardless of the solid particulate concentration. This indicates that early in the mixing process, before distributing and wetting the solid particulates, the two

Table 4  
Concentration of NaCl residues in the PCL scaffolds

Composition PCL/PEO/NaCl	[NaCl] (ppm)
25/25/50	1.6 ± 1.1
20/20/60	0.9 ± 0.8
15/15/70	11.6 ± 5.8

polymeric components go through a rapid morphological change into the co-continuous morphology. As further mixing proceeds along the screw length, the solid salt particles are wetted and the polymer blend morphology in the interstitial area is stabilized by its relative confinement. The second important observation concerning morphology development is the attrition of the salt particles. On a microscopic level, the stress that can be transferred from the melt to the solid particulates is not a function of concentration. As concentration is increased however, the contact probability between particles increases and, therefore, attrition is expected to increase. This phenomena has led to the formation of the salt bimodal size distribution shown in Fig. 8. The smaller particles that have been created by attrition are of similar size as the polymer blend segregation scale. Thus, they are easily leached with the PEO phase as shown by the residual NaCl analysis and do not interfere much with the overall pore structure. At the higher salt concentration, the remaining large salt particles have been rounded due to the important attrition leading to pores that are not as sharp as those observed at lower concentration (Fig. 5(f) vs. (d) for example). Therefore, in addition to the increased interconnectivity between large pores, increasing the salt concentration leads to a slight change in pore shape.

### 3.7. Compressive properties of the scaffolds

A key requirement for the most tissue engineering scaffolds is to match the mechanical properties of the injured tissue until the regenerated tissue takes over that specific function. Fig. 13 shows the stress–strain curves for PCL scaffolds with porosity varying between 75 and 88%. All the scaffolds were prepared with a PCL/PEO composition ratio of 50/50 except for the 88% porous sample

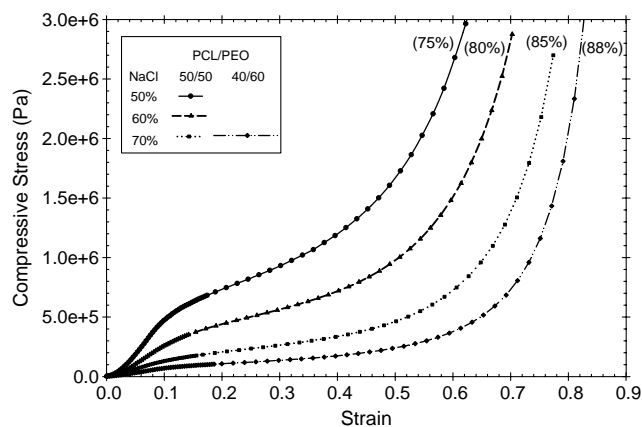


Fig. 13. Compression stress–strain curves for PCL scaffolds of different porosities. The number between parenthesis are the sample porosity. The strain rate varied from  $3.12 \times 10^{-3}$  to  $5.16 \times 10^{-3} \text{ s}^{-1}$ .

porous scaffold, which was made with PCL/PEO ratio of 40/60 to maximize the porosity. The curves corresponding to the porous PCL scaffold are typical of polymeric foam [47]. They show linear elasticity at low stresses (typically less than 10%) followed by a relatively long collapse plateau and finally a rapid increase in stress corresponding to the material densification. It is worth noting that all these PCL scaffolds can recover their deformation at strain levels higher than those corresponding to the linear elastic region. More precisely, the deformation corresponding to the plateau is still recoverable (and thus elastic) but in a non-linear fashion. In our case, this plateau is not really flat as the stress increases slightly with strain curve. This behavior is typical of closed-cell foams like those of polyethylene, due to the compression of the gas within the cells together with the membrane stresses which then appears in the cell faces [47]. It is worth noting that the later effect may prevail in our case since the interconnectivity between the pores should allow the gas to flow throughout the scaffold and eventually be expelled out, especially at the low deformation rate used for testing (between  $3.12 \times 10^{-3}$  and  $5.16 \times 10^{-3} \text{ s}^{-1}$ ). As expected, increasing the porosity of the foam decreases the compressive modulus (initial slope), decreases the plateau stress and increases the strain at which densification begins.

Fig. 14 displays the relationship between the compressive modulus and the relative density  $\rho^*/\rho_s$  of the scaffolds prepared in this study. The relative density corresponds to the porous material density divided by the pure PCL density. Compressive modulus values range from 5.3 MPa to about 1 MPa for the 75 and the 88% porous sample, respectively. More precisely, on a log–log plot, the relationship between compressive modulus and the relative density follows a power-law (i.e. linear relation on a log–log plot) as expected from the deformation mechanisms of foams model proposed by Gibson and Ashby [47]. This model assumes a cubic cell structure constructed of beams with square cross-section. According to this theoretical model, the compressive modulus is related to the relative

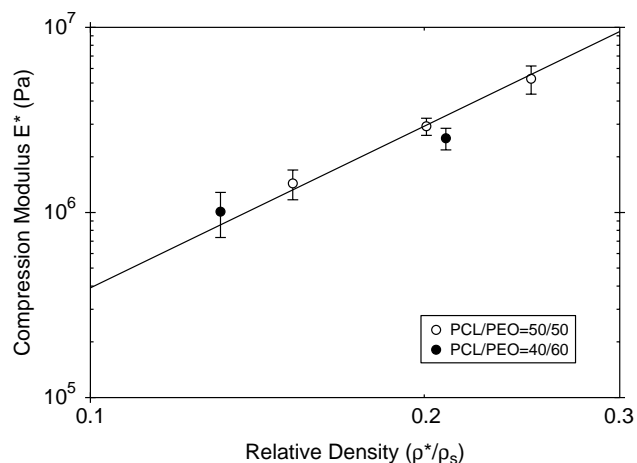


Fig. 14. Compressive modulus of PCL porous scaffolds as a function of relative density. The open and black symbols correspond to samples made with a PCL/PEO composition ratio of 50/50 and 40/60, respectively. Solid line represents the best fit for power-law equations of the form given by Eq. (4).

density of the foam by the following power-law relationship

$$E^* = c \left( \frac{\rho^*}{\rho_s} \right)^m \quad (5)$$

where  $c$  is the compression modulus of the non-porous material whereas  $m$  is the power-law exponent which should vary between 1 and 2 for an isotropic open-cell foam with uniformly distributed cells. Fitting our experimental data with this function yields  $c=313.3$  MPa and  $m=2.9$  and those results are valid over the porosity range of the data (75–88%). As shown in Fig. 14, the power-law relationship describes well the dependence of compressive modulus vs. the relative density (solid line). The estimated value of the parameter  $c$  corresponds well with the compression modulus of neat PCL ( $\cong 360$  MPa as-measured with the same set-up). However, the slope of our experimental data ( $m=2.9$ ) is higher than the theoretical range for uniform isotropic open-cell foams. Similar observations have been made for other scaffold materials. Thomson et al. [29] obtained a slope of 2.4 for a porosity range of 33–75% on PLGA scaffolds made using gelatin microspheres as a porogen agent. Hou et al. [24] obtained power-law exponents varying between 2.42 and 2.66 for PDLA and PCL scaffolds prepared by coagulation, compression moulding and salt leaching. Compression modulus measured on cancellous bone shows that data fall between lines of slope 1 and 3 [47]. This large discrepancy was explained by the different orientation of the pores, resulting in anisotropic mechanical properties. Nevertheless, the dependence of compression modulus on porosity or relative density, which is specific to the material and fabrication methods gives us the opportunity to tailor the biomechanical response of the scaffold to the damaged tissue.

Eventually, Fig. 14 shows that the compression modulus of samples prepared with a PCL/PEO composition ratio of 40/60 fall on the same modulus vs. porosity curve as the samples prepared with the PCL/PEO 50/50. Thus, at 40/60, the PCL structure retains its integrity. This is not the case for the sample with a PCL/PEO ratio of 30/70, which collapsed during extraction (not shown). This phenomenon is well illustrated by considering the PCL microstructure shown in Fig. 6 from a mechanical point of view. Decreasing the PCL content with respect to the PEO phase leads to the formation of more and more PCL short fibers and eventually droplets which do not participate to the mechanical response of the scaffold and thus weakens the porous material.

More specific compression properties have been investigated on the PCL scaffold samples by following a protocol usually applied for the measurement of mechanical properties of cartilage. It was found that the mechanical response of the sample with 85% porosity is comparable to that of a bovine cartilage with a compressive modulus of about 10 MPa. These results will be presented in separate communication [48].

#### 4. Conclusions

PCL porous scaffolds with porosity levels up to 88% and a dual pore size distribution have been obtained by a

combination of co-continuous polymer leaching and particulate leaching techniques. This technique involves the incorporation of NaCl salt particles in a co-continuous blend of PCL and PEO using melt processing techniques, followed by the selective extraction of the salt and PEO to leave a highly porous PCL scaffold. Depending on the polymers and salt concentrations, the porosity of the PCL sample can be varied between 40 and 88%. Compared to conventional salt particle leaching, this new fabrication technique allows a better control of pore interconnectivity by creation of a fully interconnected pore network. It also allows to widen the porosity range of co-continuous blend leaching technique by about 50% while maintaining good mechanical integrity. The compression modulus of the porous PCL materials was found to decrease with an increase in porosity according to a power-law relationship. The values varied from about 1 to 5.2 MPa, which may render these scaffolds suitable for load bearing applications, such as cartilage regeneration.

#### Acknowledgements

The authors would like to acknowledge the assistance of Dr Jitka Kirchnerova and Dr Pierre Sarazin, from Ecole Polytechnique de Montreal in the mercury intrusion porosimetry analysis.

#### References

- [1] Yang S, Leong KF, Du Z, Chua C-K. *Tissue Eng* 2001;7:679–89.
- [2] Huttmacher DW. *Biomaterials* 2000;21:2529–43.
- [3] Maquet V, Jerome R. *Mater Sci Forum* 1997;250:15–42.
- [4] Kim BS, Mooney D. *J Biomed Mater Res* 1998;41:322–32.
- [5] Li Y, Ma T, Yang SH, Kniss DA. *Biomaterials* 2001;22:609–18.
- [6] Mikos AG, Bao Y, Cima LG, Ingber DE, Vacanti JP, Langer R. *J Biomed Mater Res* 1993;27:183–9.
- [7] Hua FJ, Nam JD, Lee DS. *Macromol Rapid Commun* 2001;22:1053–7.
- [8] Ma PX, Zhang R. *J Biomed Mater Res* 1999;46:60–72.
- [9] Nam YS, Park TG. *Biomaterials* 1999;20:1783–90.
- [10] Schugens C, Maquet V, Grandfils C, Jerome R, Teyssie P. *Polymer* 1996; 37:1027–38.
- [11] Barry JJA, Gidda HS, Scotchford CA, Howdle SM. *Biomaterials* 2004;25: 3559–68.
- [12] Mooney DJ, Baldwin DF, Suh NP, Vacanti JP, Langer R. *Biomaterials* 1996;17:1417–22.
- [13] Sheridan MH, Shea LD, Peters MC, Mooney DJ. *J Controlled Release* 2000;64:91–102.
- [14] Gomes ME, Ribeiro AS, Malafayaa PB, Reis RL, Cunha AM. *Biomaterials* 2001;22:883–9.
- [15] Nam YS, Yoon JJ, Park TG. *J Biomed Mater Res* 2000;53:1–7.
- [16] Yoon JJ, Park TG. *J Biomed Mater Res* 2001;55:401–8.
- [17] Borden M, El-Amin SF, Attawia M, Laurencin CT. *Biomaterials* 2003;24: 597–609.
- [18] Liao CJ, Chen CF, Chen JH, Chiang SF, Lin YJ, Chang KY. *J Biomed Mater Res* 2002;59:676–81.
- [19] Schugens C, Grandfils C, Jerome R, Teyssie P, Delree P, Martin D, et al. *J Biomed Mater Res* 1995;29:1349–62.
- [20] Lam CXF, Mo XM, Teoh SH, Huttmacher DW. *Mater Sci Eng C* 2002;20: 49–56.
- [21] Tan KH, Chua CK, Leong KF, Cheah CM, Cheang P, Abu Bakar MS, et al. *Biomaterials* 2003;24:3115–23.
- [22] Landers R, Hübner U, Schmelzeisen R, Mühlaupt R. *Biomaterials* 2002; 23:4437–47.

- [23] Zein I, Hutmacher DW, Tan KC, Teoh SH. *Biomaterials* 2002;23:1169–85.
- [24] Hou Q, Grijpma DW, Feijen J. *Biomaterials* 2003;24:1937–47.
- [25] Mikos AG, Thorsen AJ, Czerwonka LA, Bao Y, Langer R, Winslow DN, et al. *Polymer* 1994;35:1068–77.
- [26] Ananthanarayan V, Shutov F. *J Appl Med Polym* 2002;6:81–6.
- [27] Iannace S, Maio ED, Nicolais L. *Cell Polym* 2001;20:321–38.
- [28] Oh SH, Kang SG, Kim ES, Cho SH, Lee JH. *Biomaterials* 2003;24:4011–21.
- [29] Thomson RC, Yaszemski MJ, Powers JM, Mikos AG. *J Biomater Sci* 1995;7:23–38.
- [30] Murphy WL, Dennis RG, Kileny JL, Mooney DJ. *Tissue Eng* 2002;8:43–52.
- [31] Ma PX, Choi JW. *Tissue Eng* 2001;7:23–33.
- [32] Tu C, Cai Q, Yang J, Wan Y, Bei J, Wang S. *Polym Adv Technol* 2003;14:565–73.
- [33] van Tienen TG, Heijkants RGJC, Buma P, de Groot JH, Pennings AJ, Veth RPH. *Biomaterials* 2002;23:1731–8.
- [34] Taboas JM, Maddox RD, Krebsbach PH, Hollister SJ. *Biomaterials* 2003;24:181–94.
- [35] Chen VJ, Ma PX. *Biomaterials* 2004;25:2065–73.
- [36] Harris LD, Kim B-S, Mooney DJ. *J Biomed Mater Res* 1998;42:396–402.
- [37] Washburn NR, Simon CG, Tona A, Elgandy HM, Karim A, Amis EJ. *J Biomed Mater Res* 2002;60:20–9.
- [38] Sarazin P, Roy X, Favis BD. *Biomaterials* 2004;25:5965–78.
- [39] Qiu Z, Ikehara T, Nishi T. *Polymer* 2003;44:3101–6.
- [40] Metzner AB. *J Rheol* 1985;29:739–75.
- [41] Elkovitch MD, Lee LJ, Tomasko DL. *Polym Eng Sci* 2000;40:1850–61.
- [42] Gubbels F, Blacher S, Vanlathem E, Jérôme R, Deltour R, Brouers F, et al. *Macromolecules* 1995;28:1559–66.
- [43] Landel RF. *Trans Soc Rheol* 1958;II:53–75.
- [44] Giesche H. Mercury porosimetry. In: Schüth F, Sing KSW, Weitkamp J, editors. *Handbook of porous solids*. New York: Wiley-VCH; 2002. p. 331–2.
- [45] Leon y Leon CA. *Adv Colloid Interface Sci* 1998;76-77:341–72.
- [46] Wardlaw NC, McKellar M. *Powder Technol* 1981;29:127–43.
- [47] Gibson LJ, Ashby MF. *Cellular solids, structure and properties*. Oxford, UK: Pergamon Press; 1988.
- [48] Gauvin C, Reignier J, Yousefi AM, Huneault M, DiRaddo R, Fernandes J. In preparation.